JOURNAL OF GEOPHYSICAL RESEARCH, VOL. 104, NO. B8, PAGES 17,633–17,651, AUGUST 10, 1999

Postglacial left slip rate and past occurrence of $M \geq 8$ earthquakes on the western Haiyuan fault, Gansu, China

C. Lasserre,[1] P.-H.Morel,[2] Y. Gaudemer,[1] P. Tapponnier,[1] F. J. Ryerson,[3] G. C. P. King,[1] F. Métivier,[1] M. Kasser,[2] M. Kashgarian,[3] Liu Baichi,[4] Lu Taiya,[4] and Yuan Daoyang[4]

Abstract. High-resolution (HR) air photographs and a 1-m horizontal and 2-m vertical resolution digital elevation model derived from them by stereophotogrammetry provide new constraints on the behavior of the western stretch of the active Haiyuan fault, in Gansu province, China. The photographs cover three swaths along the fault, each about 2-km-long and at least 500-m-wide, near the village of Songshan, at 103.5°E. This high-resolution data set is used to map and measure cumulative horizontal offsets of alluvial terraces and risers that range between 115 and 135 m, and 70 and 90 m, at two sites. Dating these terraces with ^{14}C yields minimum and maximum ages of 8400 and 7600, and 14,200 years B.P., respectively. This leads to a postglacial slip rate of 12 ± 4 mm/yr, with a most likely minimum value of 11.6 ± 1.1 mm/yr. The smallest stream offsets observed on the HR photographs range between 8 and 16 m and are interpreted as coseismic displacements of the last few earthquakes with $M \geq 8$ that ruptured the 220-km-long Tianzhu gap of the fault, west of the Yellow River. Earthquakes of that size within this gap, which has been quiescent for at least 800 years, would recur at intervals of 1050 ± 450 years.

1. Introduction

The present-day tectonic regime of the northeastern rim of the Tibet plateau is characterized by left-lateral, NE to east striking strike-slip faults and SE striking thrusts, both of which absorb NE shortening due to the India-Asia collision [e.g., *Tapponnier and Molnar*, 1977; *Tapponnier et al.*, 1990; *Gaudemer et al.*, 1995; *Meyer et al.*, 1998]. In the easternmost part of that region, the Haiyuan fault is the principal fault that accommodates the eastward component of movement between Tibet and the Gobi Ala Shan platform [*Tapponnier and Molnar*, 1977; *Zhang et al.*, 1988a, b] (Plate 1). It runs continuously for about 1000 km, from the Sulenan Shan, near 98°E, south of the Qilian Shan [*Meyer et al.*, 1998], to the western tip of the Wei He graben, north of the Qinling Shan, near 107°E [*Peltzer et al.*, 1985; *Zhang et al.*, 1995]. West of the Huang He, the fault strikes N110°E on average. East of the Huang He, it veers progressively southward to reach a strike of ~N140°E on either side of the Liupan Shan (Plate 1).

Two great earthquakes occurred on and near the Haiyuan fault, in 1920 (M = 8.7) and 1927 (M = 8 − 8.3). The former event, the Haiyuan earthquake, ruptured ~220 km of the fault [*Deng et al.*, 1986; *Zhang et al.*, 1987], mostly east of the Huang He, from 104°E to 106°E. The latter event, the Gulang earthquake [*Repetti*, 1928; *Gu et al.*, 1989] (Plate 1), northwest of the Haiyuan fault, ruptured a south dipping thrust, between 102°E and 103°E, which has been inferred to branch off this fault at depth, beneath the eastern Qilian Shan [*Gaudemer et al.*, 1995].

By contrast, the western stretch of the Haiyuan fault between 101.5°E and 104°E appears to be a major seismic gap. It is composed of three segments. The 90-km-long Leng Long Ling segment (LLL, Plate 1) is separated from the 50-km-long Maomao Shan segment (MMS, Plate 1) by the Tianzhu pull-apart basin. To the east, the Lao Hu Shan segment (LHS, Plate 1) extends ~60 km between Song Shan and Jingtai (Plate 1). Despite clear evidence of Holocene slip, there has not been one earthquake with magnitude greater than 6 along this stretch of the fault since at least 800 years [*Gu et al.*, 1989] (Plate 1). That quiescent western stretch of fault thus stands out as a likely site for future large earthquakes ($M \geq 7.5$), less than 100 km away from

[1]Institut de Physique du Globe de Paris, CNRS UMR 7578, Paris.

[2]École Supérieure des Géomètres et Topographes, Le Mans, France.

[3]Lawrence Livermore National Laboratory, Livermore, California.

[4]Seismological Institute of Lanzhou, China Seismological Bureau, Lanzhou, Gansu, China.

Copyright 1999 by the American Geophysical Union.

Paper number 1998JB900082.
0148-0227/99/1998JB900082$09.00

big cities such as Lanzhou and Xining [*Gaudemer et al.*, 1995] (Plate 1). The Holocene slip rate along this critical part of the fault was estimated by *Gaudemer et al.* [1995] to be 11 ± 4 mm/yr. This value was derived from measurements of cumulative offsets, inferred to be of postglacial age, at Sange Dun, west of the Tianzhu pull-apart (Plate 1).

A better assessment of potential seismic hazard along the Tianzhu seismic gap requires more thorough study of the fault behavior on a timescale of 10^4 years. Essential goals are to better constrain the slip rate on the fault and to determine whether the gap ruptures during characteristic earthquakes [e.g., *Schwartz and Coppersmith*, 1984] or if random behavior [*Scholz*, 1990] is more typical. To reach such goals, we performed a detailed, quantitative study of 6 km of the fault trace, near Song Shan, a few kilometers west of the 1990 $M = 5.8$ earthquake epicenter (Plate 1). High-resolution (HR) air photographs were taken using a small remote-controlled airplane, and a digital elevation model (DEM) was derived from them. At two sites, about 2 km apart, offsets of alluvial terraces were mapped and measured, using both the HR photographs and the DEM, complemented with total-station profiles. Four terraces were dated with ^{14}C from charcoal collected in trenches or in stream-cut free faces inside offset channels. Combining these measurements yields a more accurate and reliable estimate of the slip rate on the western stretch of the Haiyuan fault than hitherto available. At two other sites in between, measured offsets of order of 10 m provide plausible estimates of coseismic displacements and recurrence intervals of large earthquakes likely to have ruptured the Tianzhu gap in the past.

2. Slip Rate on the Maomao Shan Segment of the Fault

2.1. Overall Geologic and Geomorphic Setting

East of the Tianzhu pull-apart basin (Plate 1), the trace of the Haiyuan fault bounds the northern flank of Maomao Shan, a range culminating at 4074 m and exposing basement rocks [*Gansu Geological Bureau*, 1975a, b; *Xu et al.* 1989]. Farther eastward, the fault follows the Heima Zhuang He valley to a small pull-apart which formed in a ~1-km-long, left stepover on the main fault trace, north of Song Shan (Song Shan pull-apart [*Gaudemer et al.*, 1995]) (Plate 1 and Figure 1). South of the fault, the Neogene Song Shan basin is covered by loess-mantled Quaternary alluvium-forming terraces with different elevations and degrees of incision (Figures 1a and 1b). The regionally highest terraces, remnants of mid-upper Pleistocene fan systems, are capped by particularly thick loess and stand about 100 m above the basin's present-day base level (~2750 m, Figures 1b and 1c). Most of the younger alluvial terraces are incised 1–20 m by perennial streams that originate in the range north of the fault and flow into the Heima Zhuang He or feed the large fan just north of Song Shan (Figures 1a and 1b). The local yearly rainfall is of order of 300 mm/yr, typical of a mountainous continental climate, and steppe prevails. Where exposed along the edges of the Song Shan basin, the basement is chiefly composed of Silurian greenschists north of the fault and of folded Triassic sandstones south of it [*Gansu Geological Bureau*, 1975a, b]. East of the Song Shan pull-apart, the western Haiyuan fault continues across the Lao Hu Shan, slicing it into two massifs, culminating at 3222 m and 3315 m north and south of the fault, respectively. The Lao Hu Shan segment of the fault extends all the way to the Jingtai pull-apart, east of which the surface break of the 1920 earthquake stopped [*Gaudemer et al.*, 1995; *Deng et al.*, 1984, 1986] (Plate 1).

Two sites with well-preserved long-term offsets of streams and young alluvial terraces, selected on standard air photographs, one about 3 km due north of Song Shan and the other about 4 km to the northwest, on the north side of the Heima Zhuang He valley were targeted for quantitative study (sites 1 and 2, respectively, on Figure 1a).

2.2. High-Resolution Air Photographs and Digital Elevation Model

Three swaths of the topography straddling the fault, about 2 km long each, were imaged with HR photographs (Figure 1a). Sites 1 and 2 are located along the western and central swaths. The photographs were taken by a CONTAX ST 24×36 mm camera, with a ZEISS 25.9 mm focal lens, mounted in a small remote-controlled airplane (Figure 2). This plane, whose length and wingspan were 2.4 and 3.3 m, respectively, was visually guided to fly at a speed of 100 km/h, ~550 m above ground, in line with the fault. On each swath, about 36 photographs at a nominal scale of ~1/20,000, covering each an area of $\sim 500 \times 700$ m^2, with 75-80% overlap, were shot. The film was black and white Kodak TMX100. Before each flight, about ten 50-cm-square, white plastic targets were installed along each swath (Figure 2), alternatively on either side of the fault. The stereopreparation was done by measuring the positions of each target center relative to one base near the middle of the swath using a WILD (T2000, DI3000) total station. Stereophotogrammetry of the HR photographs, based on the targets coordinates, ultimately yielded a DEM, with horizontal and vertical resolutions of 1 and 2 m, respectively [*Morel*, 1995].

2.3. Measurements at Majia Wan (Site 1)

North of Song Shan, along the central swath, the fault trace strikes N100°-105°E and shows mostly horizontal displacement (Plate 2a). It runs from the base of a 2850-m-high spur (Plate 2b), above the village of Jin Tang Wa, in the west, to the west tip of the Song Shan pull-apart (Figures 1a and 1b and Plate 2a). In the

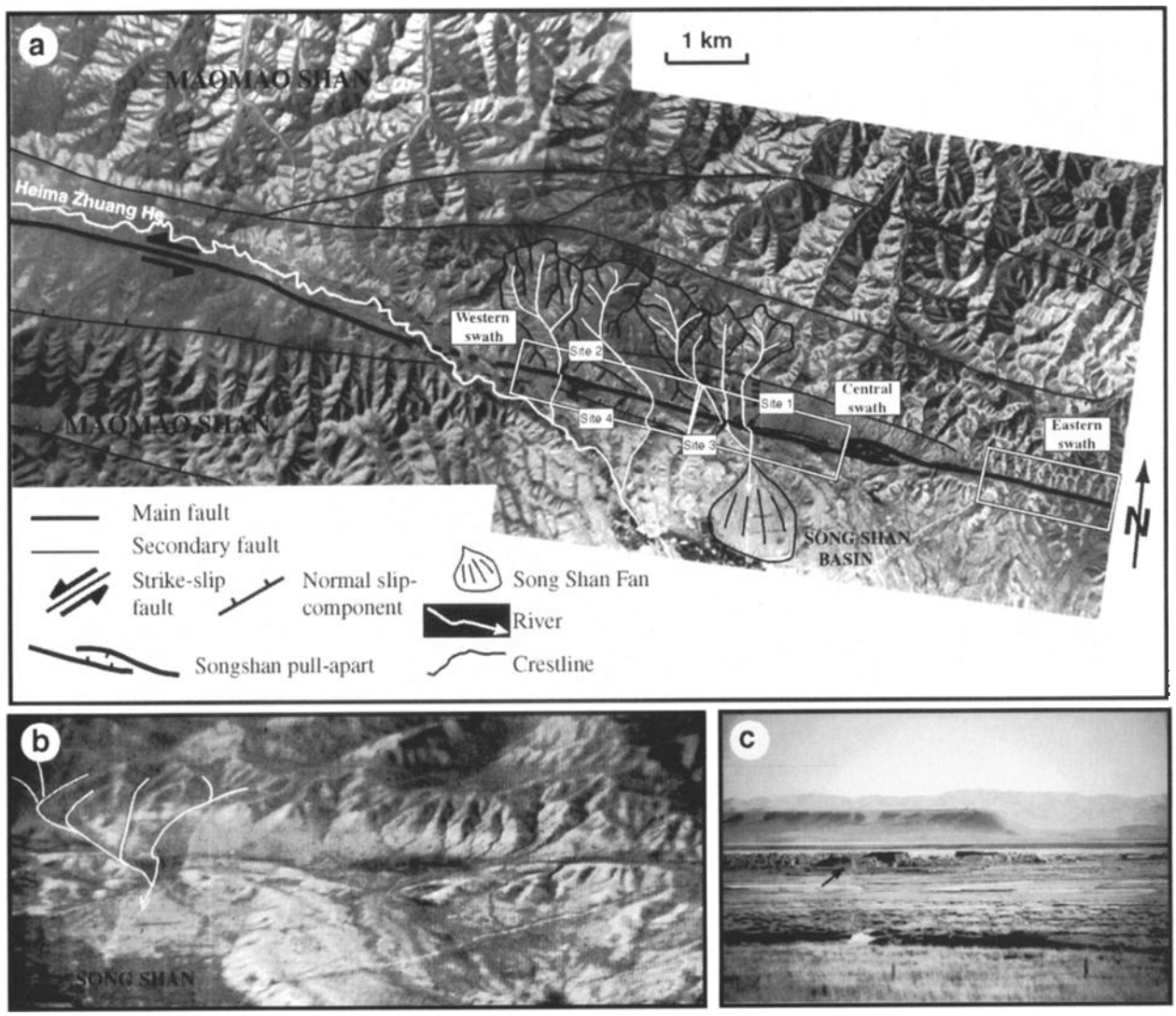


Figure 1. (a) Standard air photographs (scale 1/30,000) of Haiyuan fault near Song Shan basin. White boxes are swaths photographed by small remote-controlled airplane. Main rivers and associated catchments in area of concern are traced in white; watersheds are traced in black. Arrows indicate sites with offsets targeted in this study. Slip rates were determined at sites 1 and 2; coseismic displacements were determined at sites 3 and 4. Song Shan alluvial fan is outlined in black. Scale bar and north orientation are only indicative, due to optical distorsion. (b) Oblique north looking view of Haiyuan fault north of Song Shan. Rivers in white are those feeding Song Shan fan. Note high flat surfaces, ~50 m and 100 m above present stream level, east and west of Song Shan fan, respectively. Pull-apart in center of photograph is marked by dark, vegetated area. (c) Southwest looking view of highest (~ +100 m) loess-mantled terrace south of Song Shan basin. Arrow in middleground points to Song Shan Ming Dynasty wall, part of which collapsed during the October 20, 1990, earthquake.

western half of the swath, the fault trace cuts the channels of three south flowing streams with similar, adjacent catchments bounded, about 1.5 km north of the fault, by a WNW-ESE crest line culminating at 3050 m (Figure 1a). The two western streams meet 150 m south of the fault and join the eastern stream (Majia Wan) 200 m farther downslope, before reaching the apex of the Song Shan alluvial fan (Figures 1a and 1b). Just west of the Majia Wan stream, the fault is outlined by a narrow furrow, a few meters across, possibly deepened by human and animal passage. Eastward, this furrow gives way to a 70-m-wide, ~600-m-long depression, floored by cultivated fields, between the principal fault trace and a minor splay to the north (Plate 2a). Along this depression, both faults appear to have a component of vertical throw. The southern, principal fault strand, in particular, shows a clear north facing scarp. The south facing scarp along the northern strand is more subdued and modified by human action. That minor strand, which bears no clear evidence of horizontal slip, continues eastward toward the Song Shan pull-apart (Figures 1a and 1b), as does another strand with



Figure 2. View of small remote-controlled airplane (3.3 m wingspan) flying above steppe along eastern swath (Figure 1a), before landing. Arrow points to one target used in stereopreparation of DEM (see discussion in text). Fault trace, on left side of photograph, is outlined.

more easterly strike, yet farther north, which ultimately becomes the northern boundary of that pull-apart. We interpret the cultivated depression to have formed as a result of downthrow between the two southern strands, at the tip of the pull-apart.

Inset alluvial surfaces, incised by the three streams, are clearly offset by the principal fault strand. Our geomorphic identification of the surfaces (Plate 2c) is based on field observations (Figure 3a), on the stereoscopic analysis of the HR photographs, on the DEM (Plates 2a and 3b and Figure 3b), and on total station profiles leveled in the field (Plate 3). Though the landscape is mantled by loess, a first-order distinction and correlation between the alluvial terraces can be made according to their relative heights above the stream beds and to their relative degree of erosion and surface aspect, within the limitations discussed by *Bull* [1991] and *Merritts et al.* [1994].

Comparison between DEM profiles A and B (Plate 2b and Figure 3b) and total-station profiles SSH1–SSH5 (Plates 3a, 3b, and 3c) shows that there are four main surfaces (T1–T4) on either side of the fault, all gently sloping toward the SSE. The lowest surface level, T1, which is well developed inside the easternmost (Majia Wan) and westernmost stream channels, up to 3-4 m above the active stream beds, is clearly an alluvial terrace. T2, principally along the middle stream, is also an alluvial terrace, standing 2-3 m above T1. T3 is more thickly covered by loess and stands 2-3 m above T2. T4, which is the highest level preserved, stands 7-8 m above T3 (Figure 3a and Plate 3c). T1, T2 and T3 form relatively narrow ledges along the streams. That they are flat (Figure 3a) and slope parallel to the stream for several hundred meters (Plate 3c) corroborates a fluvial origin. T4, on the other hand, shows significant erosion and is convex upward in transverse and longitudinal sections (profiles SSH1 and SSH4 on Plates 3b and 3c). Also, it lies immediately downslope from the mountain spur to the north (Figure 1). It may thus have, in part, a colluvial-erosional origin. Finally, a minor terrace level (T1'), lower than T1, lying immediately adjacent to, and less than 2 m above, the present-day stream, is visible on the HR photographs (Plates 2c and 5) in the meanders of the stream channel south of the fault.

The best preserved terrace riser is that between T1 and T4 (called T1 riser in the following), on the right bank of the Majia Wan stream (Plates 2, 3, 4, and 5). Its offset by the fault is well recorded. The western limit of T1 along the base of this riser is well defined north of the fault, despite perturbation near the fault trace due to the presence of a small push-up. South of the fault, the gentle, slightly eroded slope between the top of T4 and the flatter surface of T1 (Plate 3e) makes it more difficult to follow the base of the riser in the field. The total-station profile SSH4 leveled along the riser base strikes N170°E north of the fault. South of the fault, it follows a straight, north striking line (Plates 3a, 3d, and 3e). We estimate the overall location accuracy of the riser base to be less than ±10 m. We cannot exclude the possibility of a slight westward deviation of

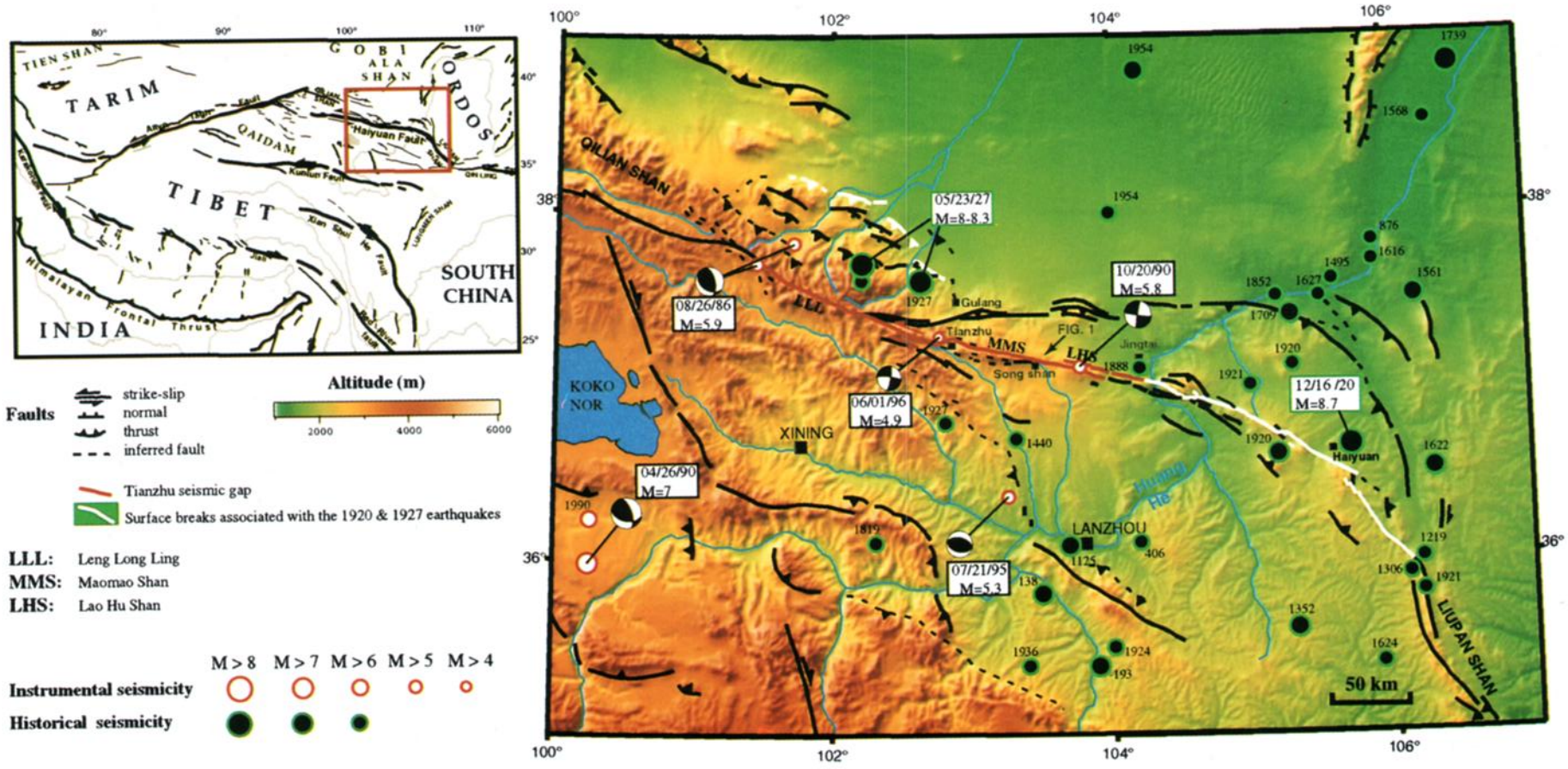


Plate 1. Seismotectonic map of Haiyuan fault system (Gansu, China). Faults and locations of historical events and of 1986 and 1990 earthquakes, as well as preferred location of 1927 earthquake, are from *Gaudemer et al.* [1995]. Tianzhu seismic gap is outlined in red. Surface ruptures associated with 1920 [*Deng et al.*, 1986] and 1927 [*Gaudemer et al.*, 1995] earthquakes are in white. Topography is from 30-arc sec Defense Mapping Agency DEM. Box in top left shows location of the Haiyuan fault within India-Asia collision zone. Arrow in center of map points to Song Shan and location of Figure 1.

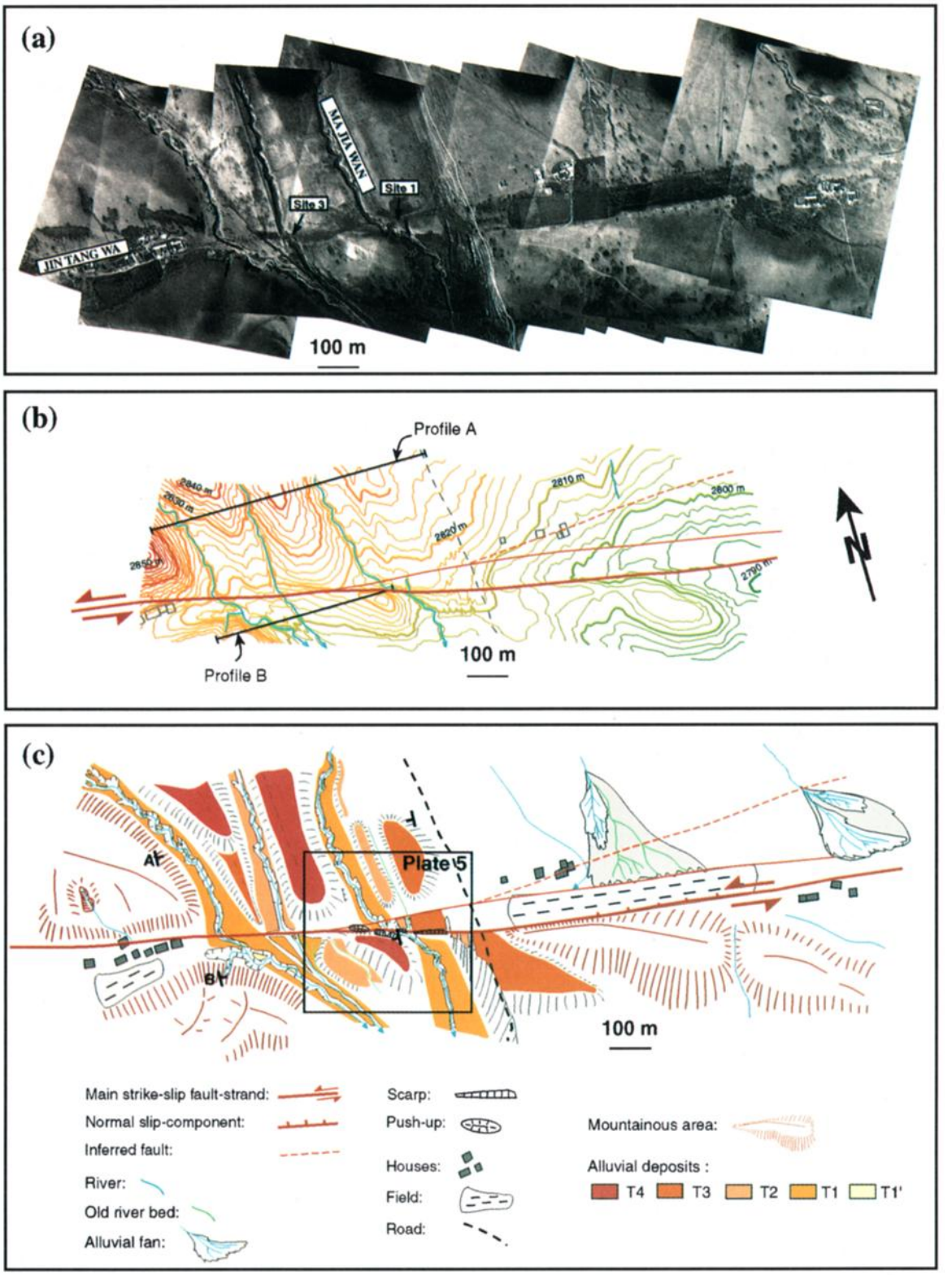


Plate 2. (a) Mosaic of high-resolution (HR) photographs of fault trace taken along central swath by remote-controlled airplane. Scale bar is only for center of each photograph. Arrows indicate locations of site 1 (Plate 3a) and site 3 (Plate 7a). (b) Digital elevation model (DEM) of central swath derived from stereoscopic analysis of HR photographs and geodetic positioning of targets installed on the ground (Figure 2). Horizontal and vertical resolutions are ~1 m and 2 m, respectively [*Morel*, 1995]. Contour interval is 2 m. Lines north and south of fault trace (red) indicate location of profiles A and B in Figure 3. (c) Geomorphic interpretation of central swath from high-resolution photos, DEM, and field observations. Four principal terrace surfaces are identified on basis of relative elevations, erosion, and surface aspect. T4 is highest and T1' is immediately adjacent to present-day stream. Box indicates location of Plate 5. Tees locate profiles A and B.

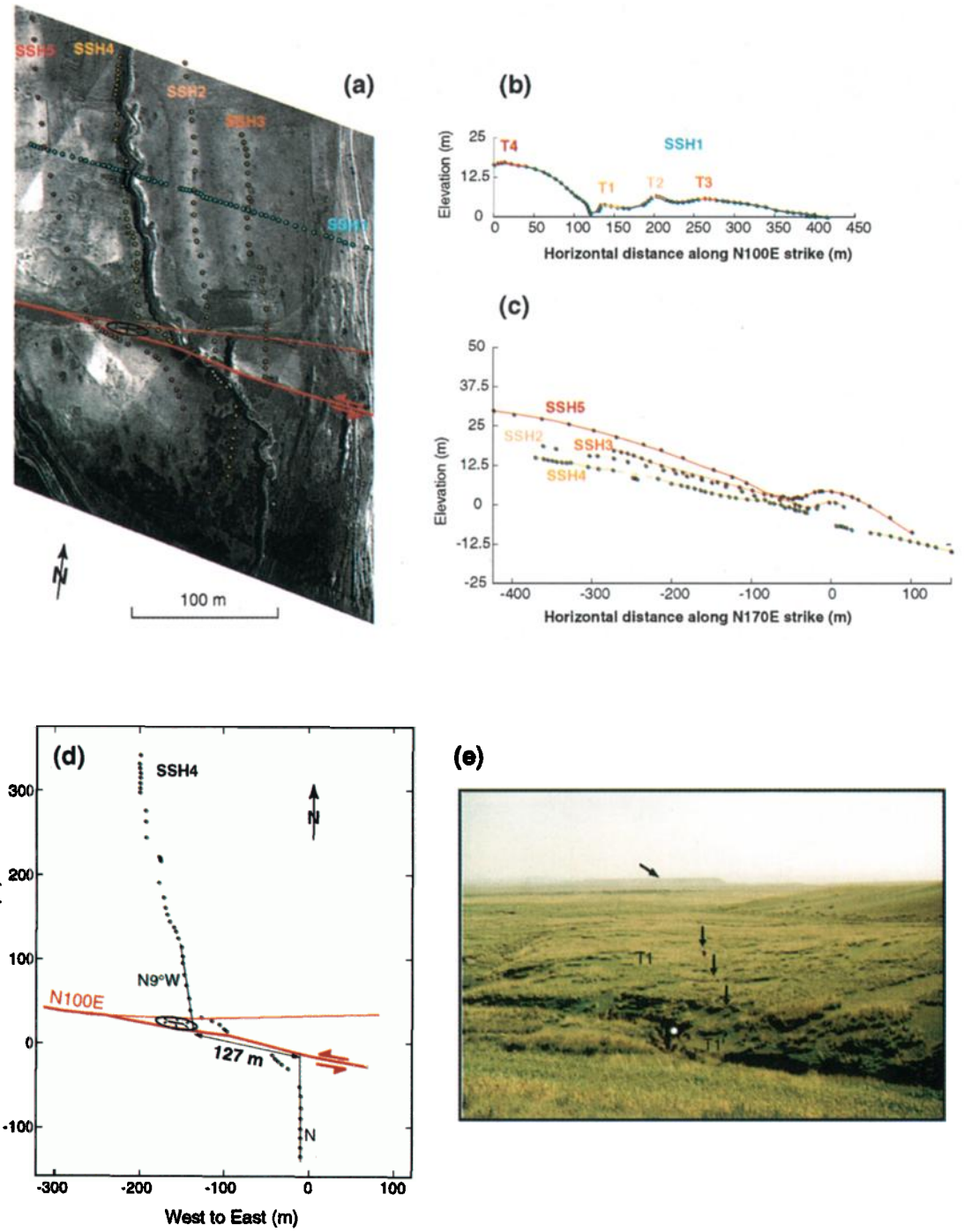


Plate 3. (a) Map view of total station profiles leveled at site 1. SSH1 (blue dots) is parallel to main fault trace (N100°E); SSH2, SSH3, and SSH5 (light orange, dark orange, and red dots, respectively) follow T2, T3, and T4 terrace ledges, respectively. SSH4 follows base of T1 riser (yellow dots). Short white dotted line, immediately south of fault, follows T1' riser (see text). SSH4 and SSH5 profiles are slightly distorted near top edge for superimposition with photograph. (b) Longitudinal profile SSH1, projected on N100°E striking vertical plane. Relative elevations of terraces are comparable to those found on DEM profiles A and B in Figure 3b. T3 appears to stand lower than T2 owing to profile strike and south slope of terrace ledges. Vertical exaggeration is 4. (c) Projections on N170°E striking vertical plane, parallel to regional slope and at high angle to fault, of total station profiles SSH2, SSH3, SSH4, and SSH5, show elevation differences between terraces. Note narrow trough of fault west of stream. Color code and vertical exaggeration are the same as in Plate 3a. (d) Map view of SSH4 profile along T1 riser. Dots are leveling points. Thick line is fault trace. Note small push-up hill near intersection between main fault trace and secondary strand splaying north. (e) South looking view of limit between T1 and gentle T1-T4 riser slope, south of fault. Arrows show N-S-striking limit followed by SSH4 profile. Red silhouette (about 1.7 m high) between arrows gives scale. Note high, mid-upper Pleistocene fan remnant in background (arrow). White dot is location of samples SSC4 and SSC5.

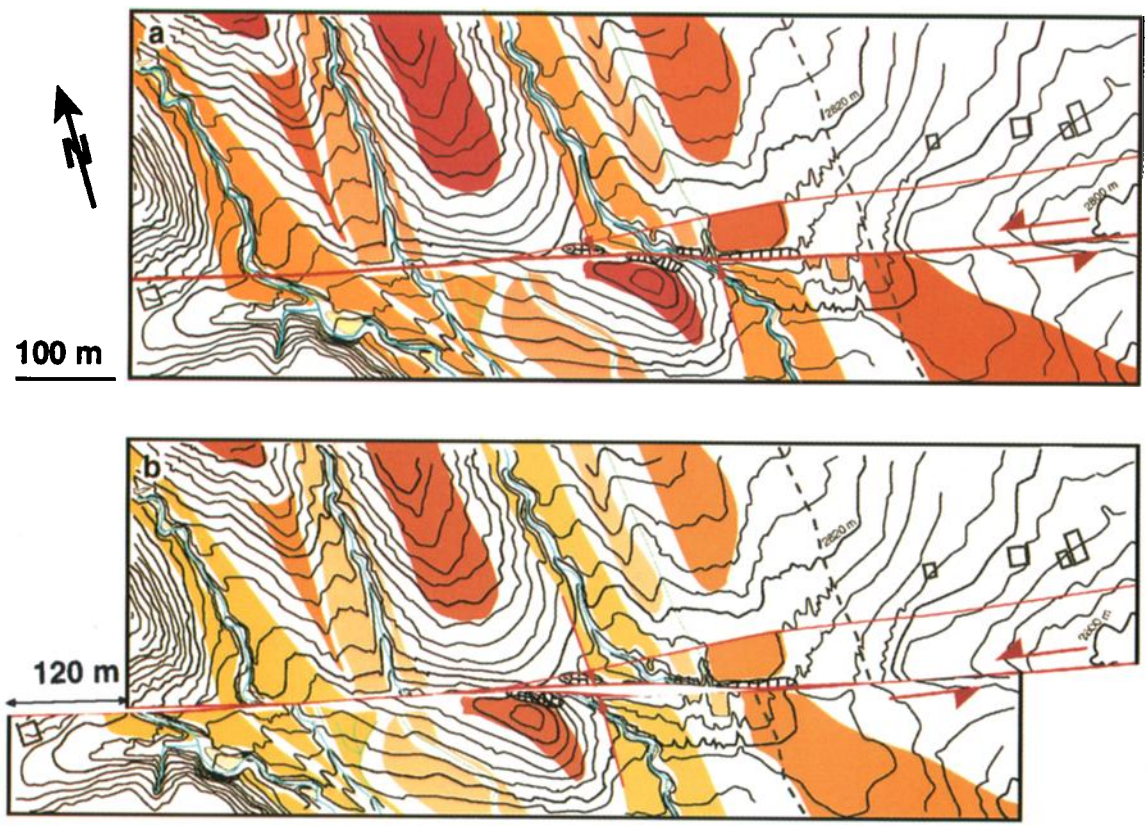


Plate 4. (a) Superimposition of terrace surfaces mapped from HR photographs and DEM. Arrows outline T1 riser north and south of fault. (b) Restoration of T1 riser and of other elements of geomorphic landscape by ~120 m displacement along fault. Same color code as in Plate 2c.

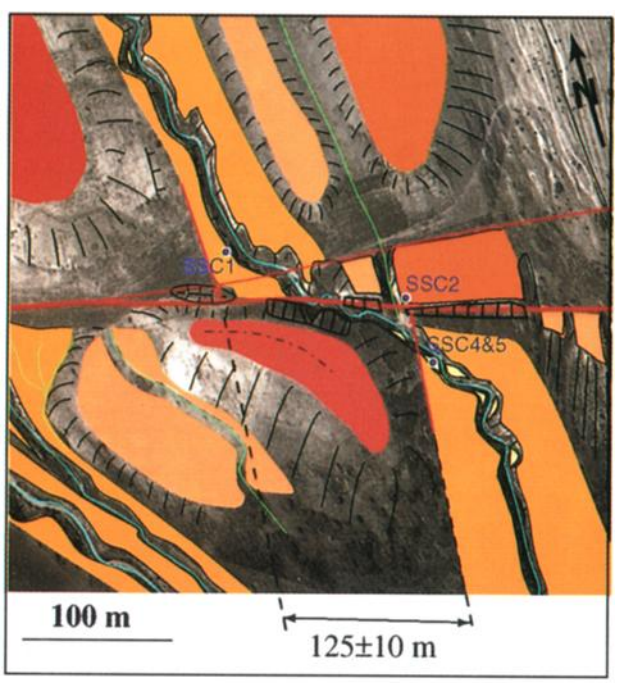


Plate 5. Map of site 1 showing locations of carbon samples and mean offset of T1 riser. Same color code as in Plate 2c.

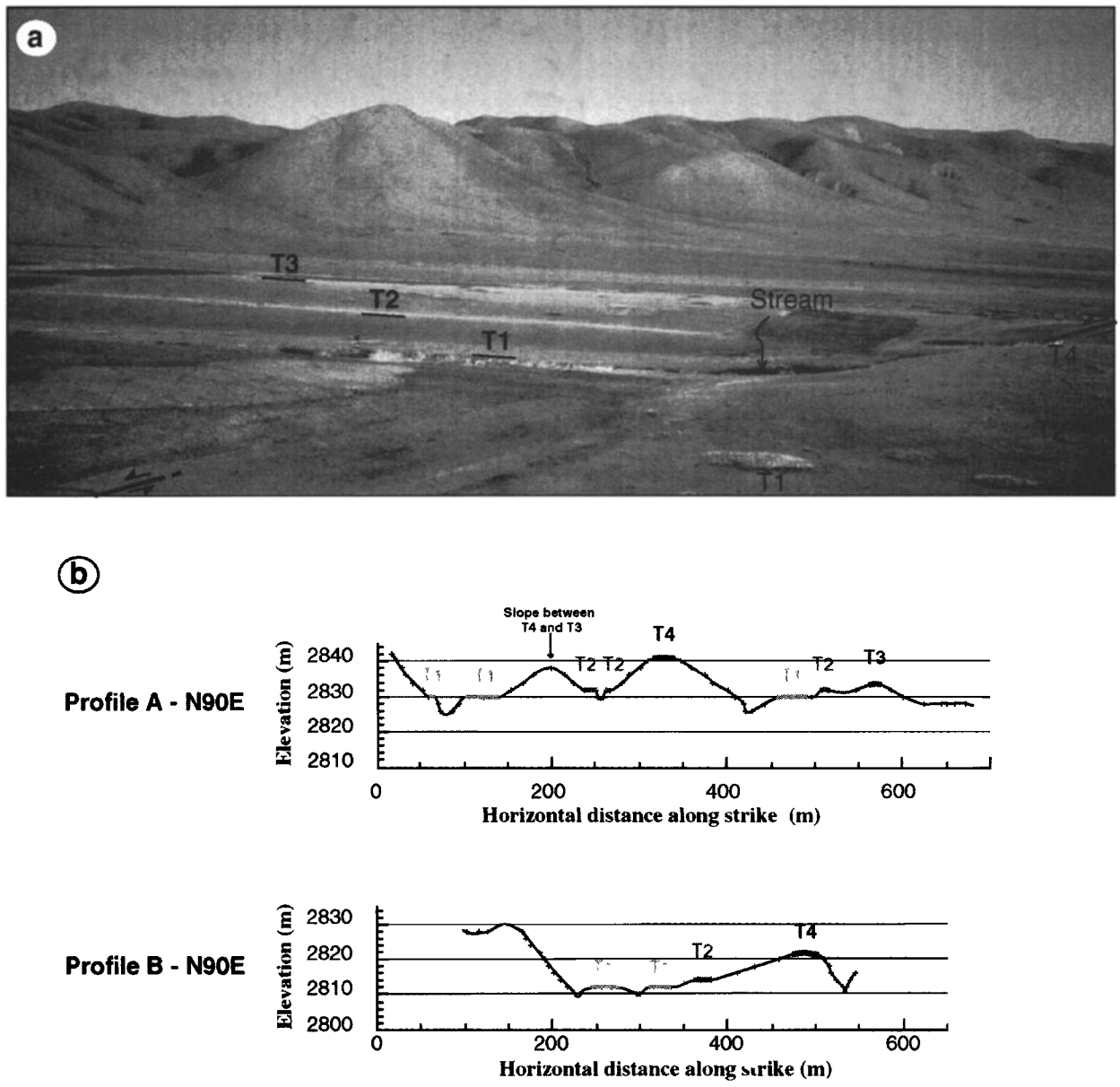


Figure 3. (a) Northeast looking view of site 1. Flat, gently south sloping terrace ledges T1, T2, and T3 are clear in middle ground, on left bank of offset stream channel. T4 is visible south of fault to the right. (b) E-W profiles, A and B, derived from vertical sections of DEM, north and south of fault, respectively (location on Plates 2b and 2c). Crosses are intersections of profile lines with contour lines of DEM. Vertical exaggeration is 4. Four different terrace levels are identified (see text).

the south part of the riser close to the fault but within the ±10 m limit. The riser offset derived from profile SSH4 is 127 m (Plate 3d). A comparable offset is obtained by reconstructing, across the fault, the original channel and terrace morphology, as constrained by superimposition of the DEM with the geomorphic map deduced from the HR photographs (Plate 4). Matching the T1 riser north and south of the fault yields an offset of 120 m. Given the uncertainties on the two measurement techniques used, we conclude that 125 ± 10 m is a reliable estimate of the T1 riser offset. This best fit also restores other channels and surfaces north and south of the fault in a consistent way (Plate 4). Emplacement of the inset terraces and incision by the streams on the south slope of the mountains north of Song Shan thus seem to have taken place in a relatively short time span. At a more detailed level, the fairly well-defined riser between T2 and T3 on the left bank of the Majia Wan stream requires about 20-25% more displacement on the fault (mean value of 150–155 m), in keeping with the fact that it is older.

In order to constrain the slip rate on the fault we sampled organic material in the alluvial deposits of three different terraces (Plate 5). The samples were dated by

accelerator mass spectrometry at Lawrence Livermore National Laboratory. All the samples ages, calibrated for ^{14}C production changes according to the method defined by *Stuiver and Reimer* [1993], are younger than 18-20 ka and thus postdate the last glacial maximum (Table 1).

The two youngest samples were collected from the lowest terrace T1', 40 m downstream from the fault, at two different depths inside the stream channel (Plates 3e and 5 and Figures 4a and 4b). Sample SSC5, composed of several charcoal pieces a few millimeters in size, was found at 65 cm depth, in a free face cut by the stream, within a soil layer containing reworked loess and clay, under a first angular gravel bed overlain by the present soil (Figures 4a and 4b). This bed corresponds to the last stream deposits before abandonment and incision of T1' [*Merritts and Vincent*, 1989]. The ^{14}C age of SSC5 (8487 ± 66 years B.P., Table 1) thus gives an upper bound to the age of abandonment of T1'. The second sample SSC4 (also charcoal) was taken 50 cm deeper than SSC5, in a comparable soil layer separated from the first one by a second angular gravel bed (Plate 5b and Figures 4a and 4b). It provides an age of 9048 ± 93 years B.P. (Table 1), older, as expected, than that of SSC5. We infer the two gravel beds to result from two flood events, probably about 600 years apart, in the pluvial period during which the bulk of T1' was emplaced. From regional studies of climatic change in northern and western Tibet this period appears to belong to the early Holocene climatic optimum (~9–6 kyr B.P.), known to have been warmer and wetter than present [*Gasse et al.*, 1991, 1996; *Van Campo and Gasse*, 1993; *Pachur et al.*, 1995; *Assaraj*, 1997; *Liu et al.*, 1998].

Other, smaller charcoal pieces were retrieved from T1 in a stream-cut face on the right bank of the river, ~25 m upstream from the fault (sample SSC1, divided in three fractions for dating, Table 1) (Plate 5b and Figures 4c and 4d). This free face shows, from top to bottom, one thin angular gravel bed under the present-day soil cover, a reworked, yellow loess layer below, then three angular gravel horizons interbedded with some lenses of reworked sand and loess, overlying a fine, loess-rich soil, where the charcoals were found at a depth of ~1.20 m (Figure 4d). The three fractions yielded comparable ages, with a mean of 9867 ± 164 years B.P. (Table 1). Again, the small gravel beds are probably related to successive floods during the more humid period

Table 1. Results of ^{14}C Dating at Sites 1 and 2 North of Song Shan

Sample Name	Fraction Modern	$D^{14}C$	^{14}C Age,[a] years B.P.	Calibrated Age,[b] years B.P.	Sample Depth, cm	Soil Type
			Majia Wan (Site 1, Central Swath)			
Terrace T3						
SSC2	0.2204±0.0022	-779.6±2.2	12150±90	14185±169	100	light colored, thick, dry loess
Terrace T1						
SSC1.1	0.3237±0.0031	-675.3±5.1	9060±160	10094±184 } 9867±164[c]	120	beige colored reworked loess under small angular pebble beds
SSC1.2	0.3364±0.0039	-663.6±3.9	8750±100	9711±177	120	
SSC1.3	0.3331±0.0020	-666.9±2.0	8830±50	9795±112	120	
Terrace T1'						
SSC4	0.3655±0.0024	-634.5±2.4	8090±60	9048±93	115	dark brown clayey sand and fine gravels under the second layer of small angular pebbles
SSC5	0.3803±0.0021	-619.7±2.1	7770±50	8487±66	65	dark brown clayey sand and fine gravels under the upper layer of small angular pebbles
			Xuanma Wan (Site 2, Western Swath)			
Terrace T1'						
PZST1	0.4262±0.0025	-573.8±2.5	6850±50	7624±43	75	thick reworked beige colored loess and sand under thin angular pebble layer

[a] Radiocarbon age using the Libby half-life of 5588 years, an assumed $\delta^{13}C$ value of -25 and following the conventions of *Stuiver and Polach* (1977).

[b] Calibration according to *Stuiver and Reimer* (1993). Mean value between lower and upper bound.

[c] Sample SSC1 divided in SSC1-1, SSC1-2, and SSC1-3 in laboratory. Mean value of the three calibrated ages given.

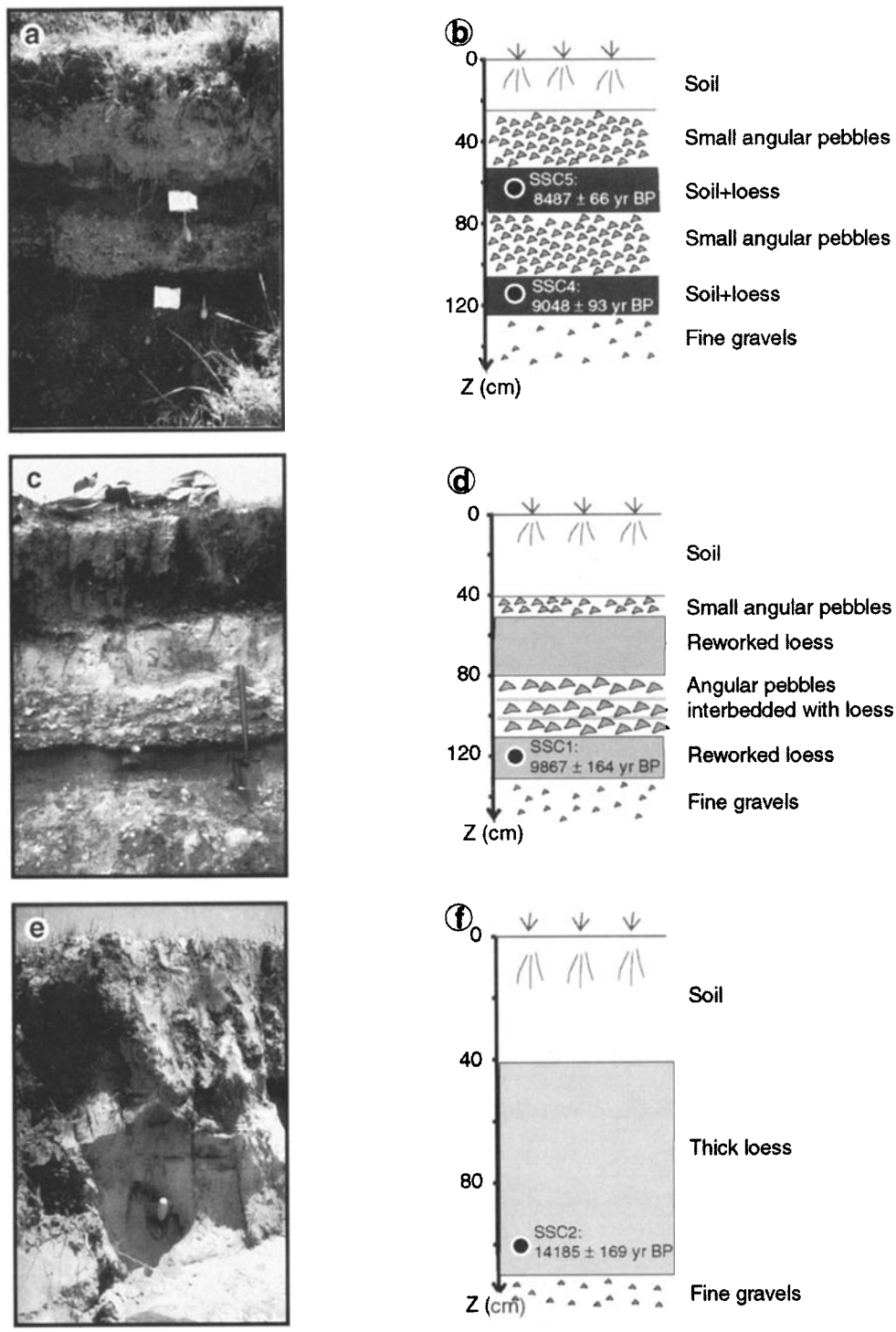


Figure 4. Photographs and corresponding sketches of erosion-cut free faces from which charcoal samples were collected. (a) and (b) SSC4 and SSC5, (c) and (d) SSC1, and (e) and (f) SSC2 samples.

that postdated the beginning of the Holocene [*Gasse et al.*, 1991, 1996]. However, we lack information about the time that elapsed between deposition of the three lower gravel layers and the upper one, and hence between the age of SSC1 and the actual age of complete abandonment of T1, which might be significantly younger than 9900 years B.P. (Figures 4c and 4d).

Finally, one small sample (SSC2) was collected from T3, north of the fault, from an erosional cliff that we cleaned off (Plate 5). Here a single, tiny piece of charcoal was found immediately above a layer of thin gravel capping the terrace, at the base of a thick, dry layer of loess underlying the present soil (Figures 4e and 4f). The 14,185±169 years B.P. obtained (Table 1) provides

a lower bound to the age of abandonment of T3 [*Weldon*, 1986; *Personius*, 1995; *Merritts et al.*, 1994]. Overall, all the ^{14}C ages at site 1 are thus consistent with the relative heights of the terraces above the stream bed, a higher terrace giving an older ^{14}C age (Table 1).

2.4. Measurements at Xuanma Wan (Site 2)

On the westernmost swath imaged by the plane, north of the Heima Zhang River, the fault trace, marked by a prominent slope break, strikes N100°-105°E, along the base of faceted spurs (Figure 1a and Plate 6a). South of the fault, and parallel to it, a 200–300-m-wide corridor, floored by flat, broad terraces, separates the Maomao Shan range front from a string of hills capped by mid-upper Pleistocene fanglomerates overlain by thick loess, pitted with numerous karstic dolines (Plate 6a and Figure 5). Small rills flowing down the facets, and two streams with larger watersheds in the Maomao Shan to the north, incise the terraces (Plate 6a). These streams have catchments areas comparable to those of the central swath streams, adjacent to the east (Figure 1a). Both the western (Xuanma Wan) and eastern streams flow into the Heima Zhuang River, with which they merge 500 and 1500 m south of the fault, respectively. This river flows southeast across the Song Shan basin toward the Huang He (Plate 1 and Figure 1a).

Site 2 is located where the Xuanma Wan stream course is offset by the fault (Plate 6a and 6b). Across the corridor following the fault, this stream incises, by up to 20 m, three alluvial terraces of different elevations that dip gently toward the south (Plate 6c and Figures 5a and 5b). Because of strong winds during the flight, erratic tilt and altitude and direction changes of the plane prevented DEM reconstruction. However, from the relative heights of the terraces above the stream and their geomorphic aspect in the field, we infer that they correlate roughly with T1', T1, and T4 at site 1, in order of increasing elevation (Plates 5 and 6c). Such a correlation is plausible since the streams at both sites have similar catchments only 2.5 km apart on the same flank of the mountain range (Figure 1a) [*Bull*, 1991]. It is also in keeping with the inference that the emplacement and abandonment of the terraces were orchestrated by regional climatic change, whether along the Haiyuan fault [*Gaudemer et al.*, 1995] or elsewhere in north central China [*Peltzer et al.*, 1988; *Avouac et al.*, 1993; *Meyer et al.*, 1996; *Van der Woerd et al.*, 1998].

The base of the best preserved and highest riser, between T4 and T1', on the right bank of the stream, is cleanly offset 80 ± 10 m by the fault (Plate 6c and

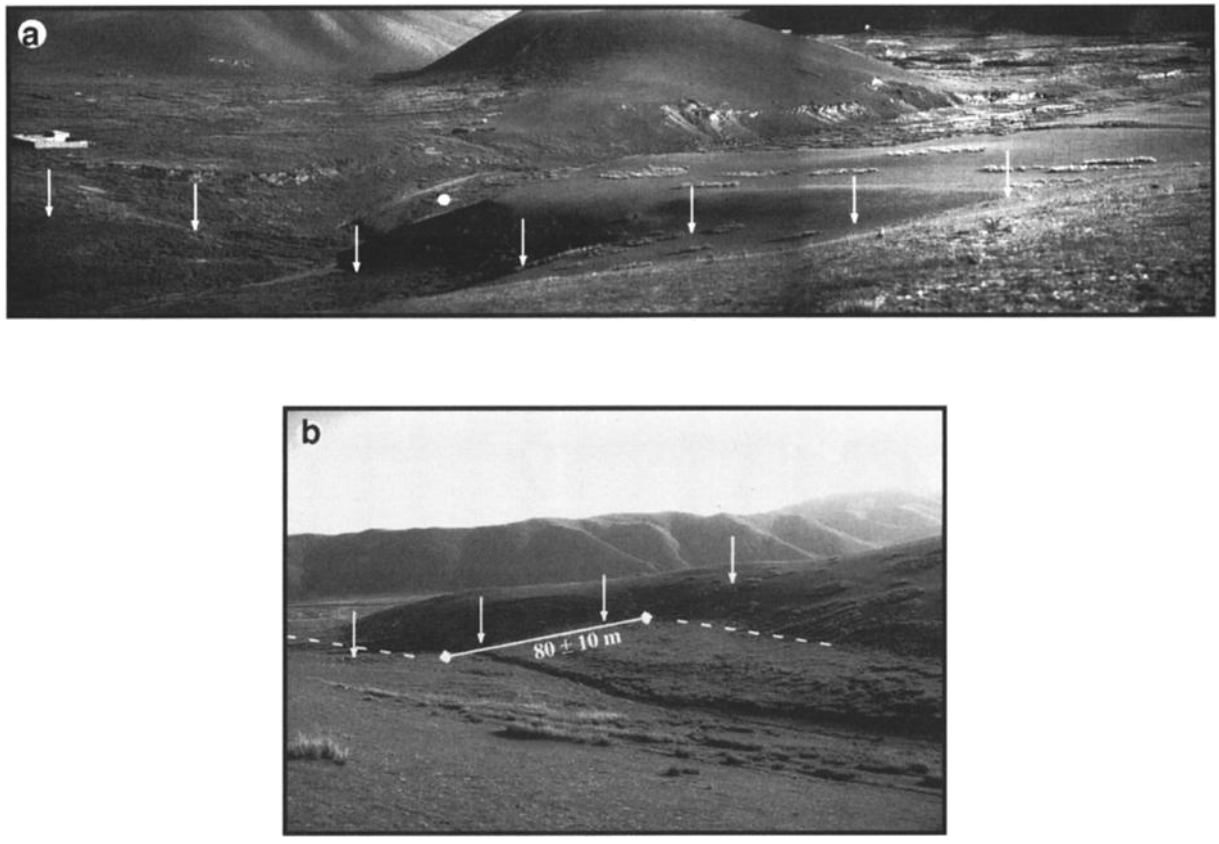


Figure 5. (a) Southeast and (b) southwest looking views of T4-T1' riser offset. Note how clean cut and clear this offset is. White dot is location of sample PZST1. White arrows indicate fault trace.

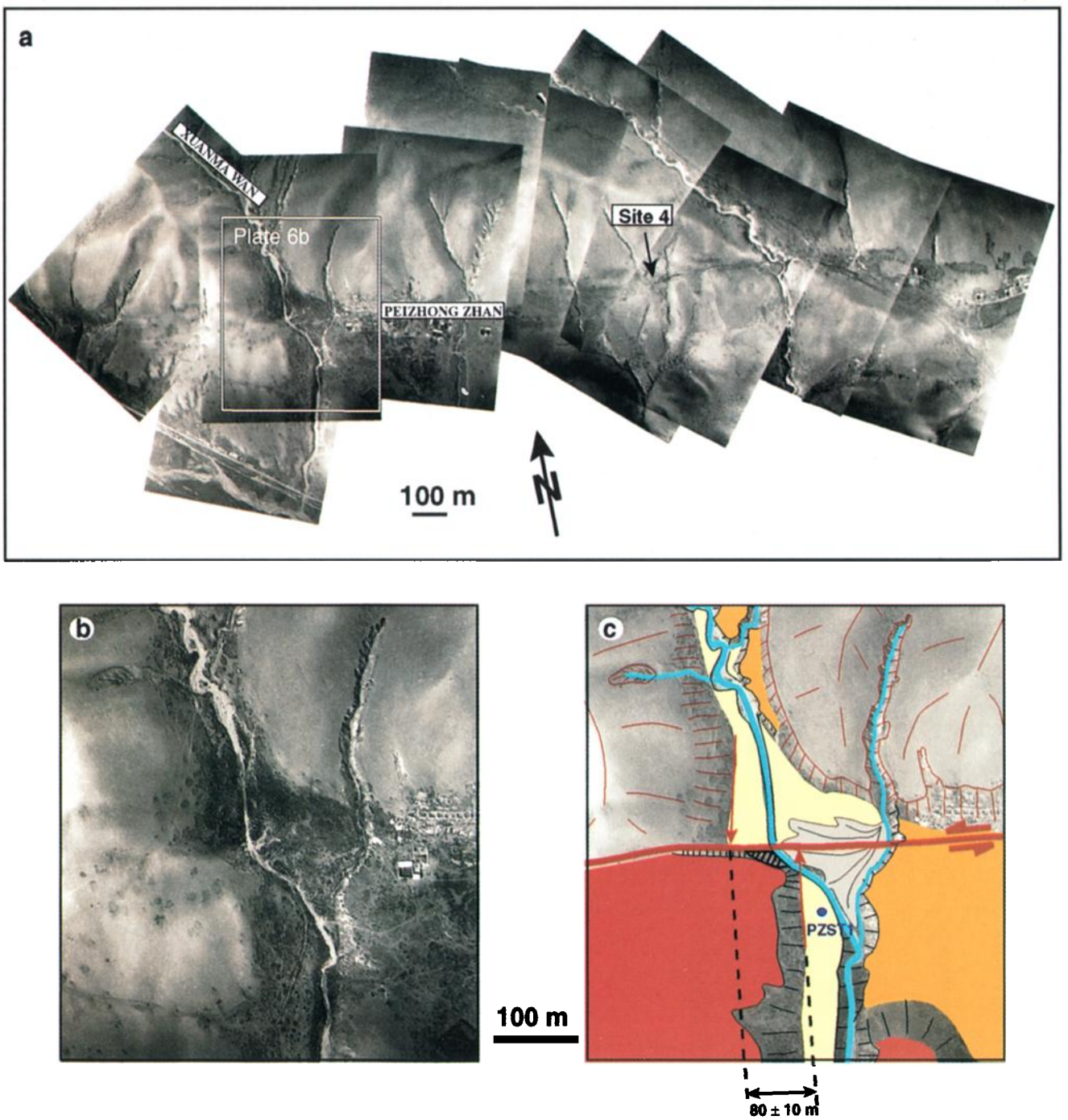


Plate 6. (a) Mosaic of high-resolution photographs of western swath. Note erratic orientation of photos. Scale bar is only for centers of photos. Box shows location of Plate 6b (site 2) and arrow shows location of Figure 7 (site 4). (b) Enlargement of HR photograph of site 2 and (c) geomorphic interpretation. Terraces roughly correlate with those at site 1 (see Plate 2a). Color code is identical. Arrows indicate T1' riser base north and south of fault, used to measure 80 ± 10 m offset. Black dot south of fault indicates location of trench in which PZST1 carbon sample was found.

Figures 5a and 5b). This offset is smaller than the 125 ± 10 m T4-T1 riser offset at site 1, in keeping with our terrace correlation between the two sites. It is only derived from the analysis of HR photographs, however, without accurate topographic constraint.

We could retrieve only one charcoal sample at this site, from a trench dug into T1', at the foot of the T4-T1' riser, 75 m south of the fault, on the right bank of the stream (Plate 6c). This sample (PZST1, after Peizhong Zhan village nearby), taken at a depth of 70 cm in a loess-rich soil layer under a thin, angular gravel bed below the present soil (Figures 6a and 6b), yielded an age of 7624 ± 43 years B.P. (Table 1), which provides an upper bound to the age of abandonment of T1'. This age implies that the terrace identified as T1' at site 2 might be ~800 years younger than T1' at site 1 (Table 1). Comparison of the corresponding subsurface logs (Figures 4b and 6b) does reveal differences in the stratigraphy. The top gravel bed is thinner at site 2 than at site 1, while the underlying loess layer is thicker. Such differences probably reflect the variance of bed thickness generally observed along small streams.

2.5. Constraints on the Left-Lateral Slip Rate

The reliability of slip rate determination from measurement of a terrace riser offset depends on the way in which the riser has recorded the offset and on the age attributed to that offset. Degradation of a riser, depending, for instance, on incision rate, can affect a terrace riser shape and slope, leading to large uncertainties in offset measurement [*Weldon*, 1986; *Bull*, 1991; *Merritts et al.*, 1994; *Gaudemer et al.*, 1995]. The offset age is commonly taken to be that of abandonment of the terrace at the base of the riser. Indeed, a riser is assumed to be constantly rejuvenated by flow while the stream runs along its base and to start recording offset by a fault only after the stream bed at its base is completely abandoned, forming a new terrace [*Weldon and Sieh*, 1985; *Bull*, 1991; *Avouac et al.*, 1993; *Gaudemer et al.*, 1995; *Van der Woerd et al.*, 1998]. This scenario is widely accepted for strath or fill-cut terraces, since lateral bank erosion constantly rejuvenates risers. In the case of fill terraces, however, whose deposition can postdate previous incision and lateral shaping of older risers, a riser offset can be older than the end of the filling event [*Bull*, 1991].

At site 1 the basement upon which the alluvium rests is not exposed. Hence, whether the terraces are straths is uncertain. Given the proximity and small surface of the Majia Wan stream drainage catchment (less than 1 km^2) and the small size of the angular gravels observed in the free face cut into T1, upstream from the fault (Figure 4d), one might doubt that the river once had enough power to erode both laterally and vertically, and that T1 was a strath. Site 1, however, is about halfway between the upper catchment of the stream in the Maomao Shan and the Song Shan fan. The area of dominant deposition thus lies farther downstream, while erosion and transport, both of which are characteristic of strath formation, must be important along the channel crossed by the fault, especially during floods, in keeping with the flatness of the base of the gravel layers, as well as with their small thickness. Finally, the overall asymmetry of deposition along the stream implies predominant erosion and rejuvenation of risers on its right bank. The stream presently flows closer to the T1 riser on the right bank and has deposited unpaired older terraces along its left bank (T2, T3, Plate 2c). This probably results from the SW trend of the stream course farther upslope (Figure 1a). As the stream veers to a N170°E direction, preferential lateral erosion occurs on its right bank, as if T1 were a strath. Thus we find it likely that the straight geometry of the T4-T1 riser on the west side of the Majia Wan stream channel was shaped by lateral erosion until this stream abandoned T1. In keeping with this inter-

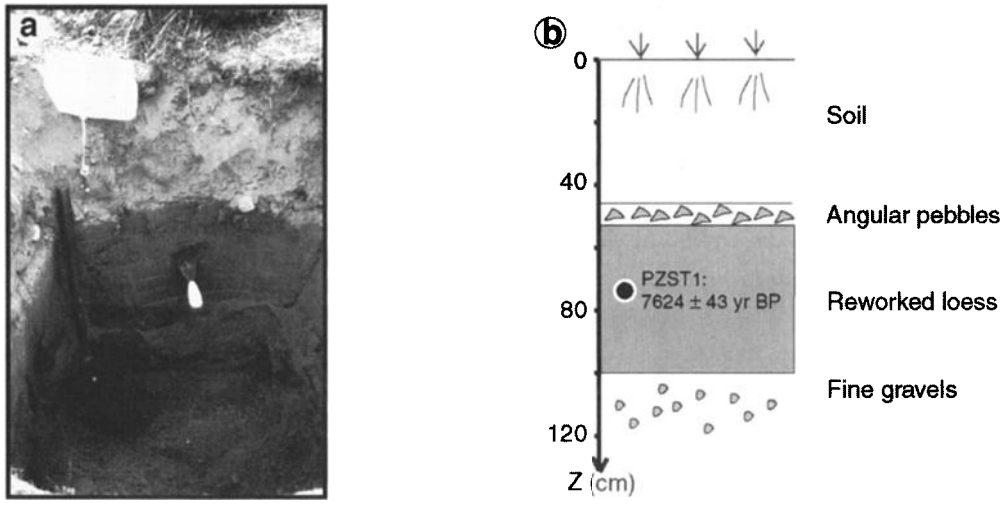


Figure 6. (a) Photograph and (b) corresponding sketch of trench in which PZST1 sample was collected.

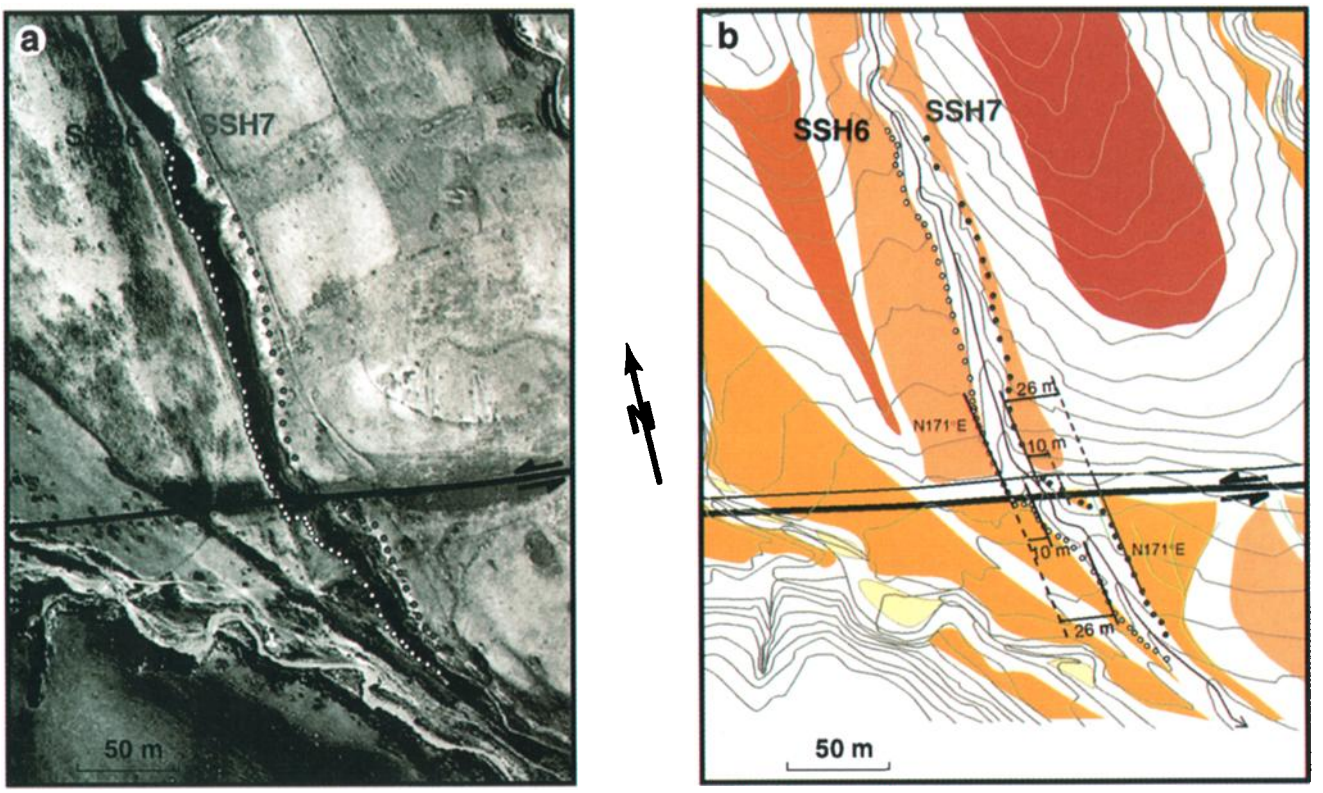


Plate 7. (a) HR photograph of small-scale offsets at site 3 (Figure 1a and Plate 2a) on central swath. (b) Map view of profiles leveled, plotted on DEM (color code as in Plate 2c). Profiles SSH6 and SSH7 follow offset stream channel risers on right and left banks, respectively. Dark line indicates fault trace.

pretation, 125 ± 10 m of cumulative displacement would have accrued on the fault since the abandonment of T1. As sample SSC1 provides an upper bound to the age of abandonment (9867 ± 164 years B.P., Table 1), the lower bound of the slip rate on the Haiyuan fault at Majia Wan site would be 12.7 ± 1.2 mm/yr. Although a curved T1 riser shape south of the fault cannot be excluded, suggesting deposition of T1 in an already deviated channel, hence a long-term offset somewhat smaller than that measured, the 10-m uncertainty on that offset includes such a possible deviation.

In any case, overall reliable bounds on the rate can be derived from the ages of the other two terraces that were dated. The cumulative 125 ± 10 m offset is likely to postdate the abandonment of T3, whose age must be older than that of SSC2 ($14,185 \pm 169$ years B.P., Table 1 and Plate 5b and Figure 4f) and must predate deposition of T1' and hence 8487 ± 66 years B.P., age of SSC5 (Table 1 and Plate 5b and Figure 4b). The corresponding lower and upper bounds on the slip rate are therefore 8 and 16 mm/yr, respectively (mean of 12 ± 4 mm/yr).

Site 2 (Plate 6) yields another independent estimate of the slip rate. In contrast with the situation at site 1, T1' and T1 are seen to rest flat on abraded basement upstream from the fault and clearly have a strath origin. Moreover, as the T4-T1' riser is well defined, straight, and cleanly cut by the fault both upstream and downstream from it (Plates 6b and 6c and Figure 5), one may safely assume that it kept being shaped by lateral erosion as long as the Xuanma Wan stream kept flowing on T1'. The 80 ± 10 m offset of that riser was thus recorded after abandonment of T1', whose maximum age is 7624 ± 43 years B.P. (sample PZST1 on Figure 5). This provides a lower bound of 10.5 ± 1.4 mm/yr on the slip rate at Xuanma Wan, consistent with the bounds found at the other site. Such redundancy leads us to conclude that the slip rate on the Maomao Shan segment of the western Haiyuan fault near Song Shan lies reliably between 8 and 16 mm/yr. At a more refined level of analysis the minimum value we find most plausible, considering both sites, is 11.6 ± 1.1 mm/yr (mean value of 12.7 ± 1.2 and 10.5 ± 1.4 mm/yr).

3. Coseismic Offsets of Large Earthquakes in the Tianzhu Gap

The HR photographs draw attention to two other sites where minimum offsets on order of 10 m are visible along the fault (sites 3 and 4 on Figure 1a). Site 3 is located just west of the long-term offset at Majia Wan, where the fault trace cuts the channel of the middle stream (Figure 1a and Plates 2a and 7a). Here, the river incises T2, north of the fault, by 3–4 m and T1,

south of the fault, by less than 2 m (Plate 7b). Both the western and eastern risers of the stream channel are offset by the fault. To measure such offsets with an accuracy of less than 1 m, we leveled two total-station profiles [e.g., *Gaudemer et al.*, 1995] along the tops of the two risers (Plates 7a and 7b).

Upstream from the fault, the western riser top is sharply defined, with a strike of N171°E. Its piercing point can be located precisely (Plate 7b). From the geometry of the channel downstream, two offsets of different ages can be identified. The smallest and most recent one, measured at the fault trace, is 10 m. A larger, more ancient, cumulative offset of 26 m is measured between the riser north of the fault and the segment of that riser that has the same trend (N171°E), 30 to 70 m south of the fault (Plate 7b). Farther south, the middle stream turns toward the SE and merges with the western stream (Plate 2a).

North of the fault, meandering of the stream has degraded the eastern riser, which is less straight and sharp than the western one, particularly near the fault (Plate 7a). Given the fairly constant width of the channel (~18 m), however, we assume that this upstream riser had the same trend as the western riser near the fault (Plate 7b). South of the fault, the eastern riser first bounds a small, triangular-shaped patch of T1, separated from the rest of T1 to the east by a dry, beheaded stream bed (Plate 7b). Farther south, it then resumes a well-defined, N171°E strike, in continuity with this dry stream bed. The cumulative offset between the best defined segments of the eastern riser north and south of the fault is 26 m, identical to that of the western riser (Plate 7b). A more questionable offset of ~10 m is apparent between the extrapolated extension of the eastern riser just north of the fault and the western edge of the small T1 triangle south of the fault (Plate 7b). This offset is also identical to the smallest offset of the western riser.

Hence two sets of identical offsets (10 m, 26 m) are measured at site 3, using both the western and the eastern risers of the stream channel cut by the fault. The larger one is 2–3 times the smaller one. Since the 10 m offset is the smallest observed on the central swath, we interpret it to be close to the coseismic displacement of the last earthquake on the fault at this site. In keeping with this interpretation, the 26 m offset might represent the cumulative displacement of the last two, or perhaps three, earthquakes on the fault.

The second site (site 4) is located between the two main streams of the western swath (Figure 1a and Plate 6). West of the eastern stream, two small rills that flow down the faceted spur, with headwaters only ~200 m north of the fault (Plate 6a), show cumulative offsets of 80 ± 20 m on the HR photographs (Figure 7). The uncertainty on the offset measurement comes from the sigmoidal bend of the rills as they cross the fault and from their significantly different strikes on either side of the fault, N174°E to the north and N12°E to

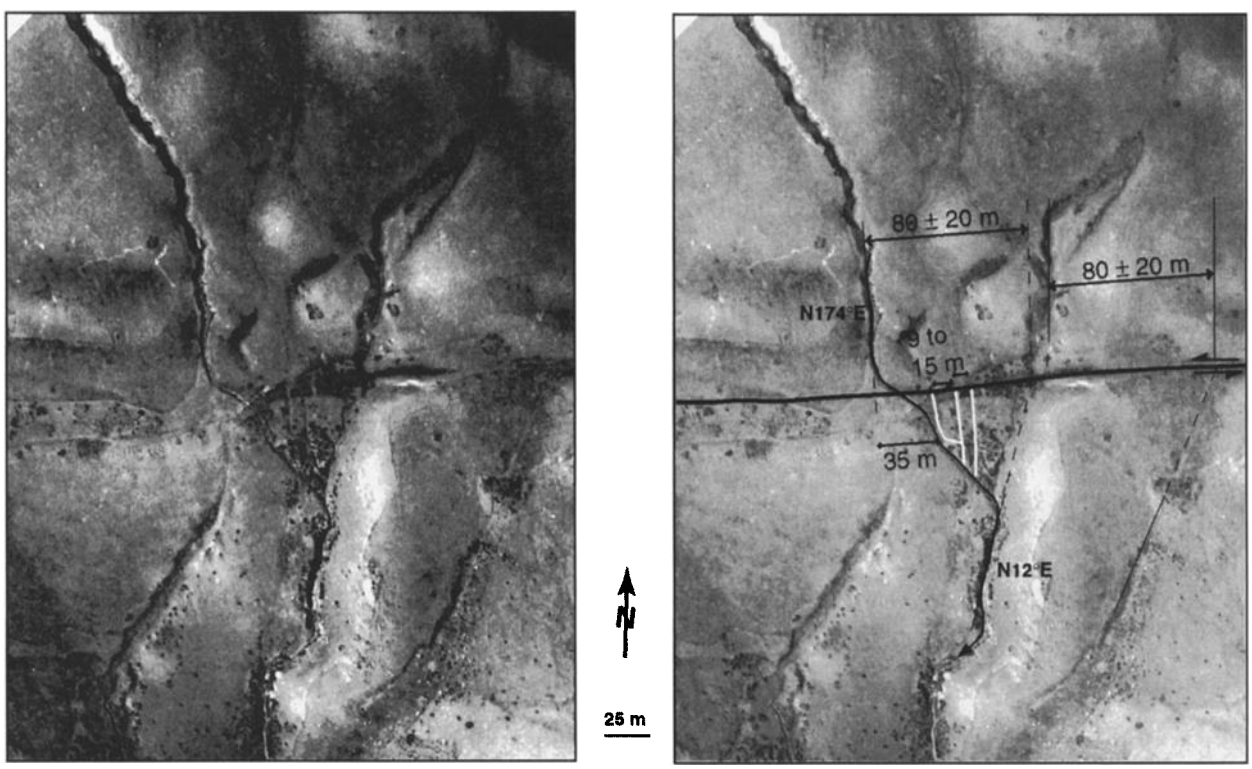


Figure 7. Enlargement of HR photograph at site 4 (western swath, Figure 1a and Plate 6a) showing cumulative offsets of two rills and of three beheaded channels south of fault trace, spaced 9 to 15 m. Smallest offsets are interpreted as coseismic displacements during past large earthquakes (see discussion in text).

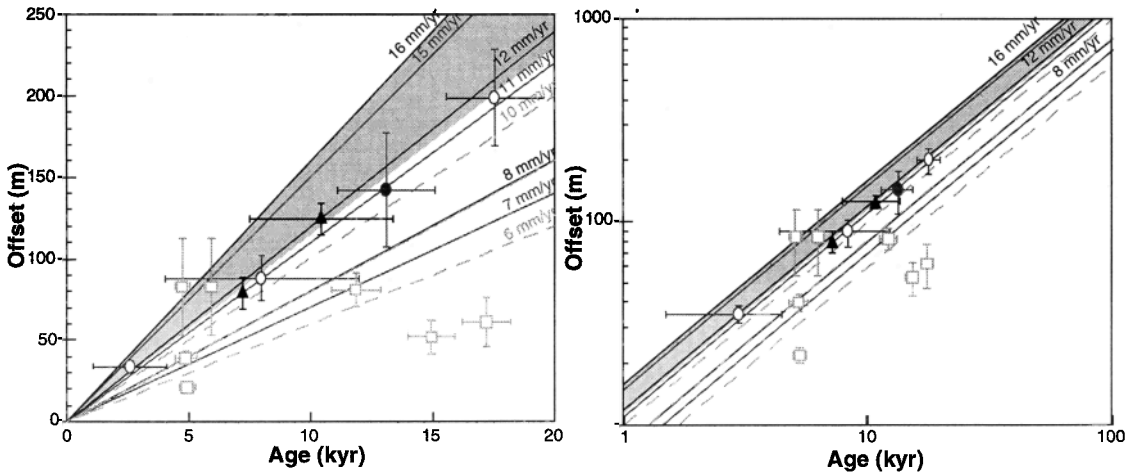


Figure 8. Summary plots of cumulative offsets on Haiyuan fault as a function of their ^{14}C or inferred ages, on linear and logarithmic scales. Squares are values from *Zhang et al.* [1988a], ellipses are values from *Gaudemer et al.* [1995], and triangles are values from this study. Bars are uncertainties. The 8 ± 2 mm/yr value is lower bound of slip rate east of Huang He [*Zhang et al.*, 1988a]. The 11 ± 4 mm/yr value is slip rate at Sange Dun, west of Huang He, based on ages inferred from postglacial warming [*Gaudemer et al.*, 1995]. Results of our study (12 ± 4 mm/yr), based on ^{14}C dating, are consistent with latter rate. Shaded zone is range of preferred slip rate value (see text).

the south, respectively. Recall that no DEM is available on this swath. Note, however, that the long-term cumulative offsets of the rills are similar to that of the Xuanma Wan stream (Plates 6b and 6c).

Smaller offsets of the western rill also exist at this site, within the triangular confluence area south of the fault at the center of the photograph (Figure 7). Here three small beheaded channels that trend parallel to the main rill north of the fault are clear from stereoscopic analysis of the HR photographs (Figure 7). All these channels, whose piercing points are well defined, lie east of the intersection between the fault and the main rill. The present-day rill channel is offset about 35 m by the fault. The spacing of the three beheaded channels to the east is 9 to 15 m. Interpreting these channels as abandoned courses of the main western rill, with increasing ages toward the east, suggests a succession of consecutive earthquakes with coseismic displacements ranging between 9 and 15 m each, consistent with those observed at site 3.

Short-term offset measurements at sites 3 and 4 thus suggest that slip amounts (Δu) of past seismic events on the western Haiyuan fault near Song Shan were between 8 m and 16 m (mean $\Delta u = 12 \pm 4$ m). Each event would therefore have reached a magnitude $M_w \geq 8$, if they ruptured a 20-km-thick seismogenic crust over the entire length of the Tianzhu gap (220 km [*Gaudemer et al.*, 1995]). Such a rupture length and slip amount are compatible with scaling laws [e.g., *Wells and Coppersmith*, 1994].

4. Discussion and Conclusion

The long-term riser and channel offsets measured with HR photographs at the Majia Wan and Xuanma Wan sites and at site 4 near the eastern tip of the Maomao Shan segment of the western Haiyuan fault (125 ± 10 m, 80 ± 10 m, 80 ± 20 m) and the ^{14}C ages of the inset terraces (14.2, 9.9, 9, 8.5, and 7.6 kyr B.P., Table 1) constrain both the main landscape-shaping epoch north of Song Shan and the postglacial left slip rate on the fault.

Our results are consistent with those of the larger scale study performed by *Gaudemer et al.* [1995]. These authors documented left-lateral offsets of terrace risers, stream channels, crest lines, and glacial valley edges in Leng Long Ling, near the Tianzhu pull-apart basin, and along the Lao Hu Shan (Plate 1). They noted the consistency of such offsets along the entire 220 km length of the western stretch of the Haiyuan fault. The long-term offsets of 80 ± 10 m and 125 ± 10 m we measured near Song Shan fit with the clustering of offsets they obtain [*Gaudemer et al.*, 1995, Table 1 and Figures 6 and 14]. Lacking absolute ages of the offset morphological markers they measured, *Gaudemer et al.* [1995] inferred their formation to be related to climatic change, particularly to the last glacial maximum (20–18 kyr B.P.), the deglaciation (15–11 kyr B.P.), and the early Holocene climatic optimum (9–6 kyr B.P.). Such inferences are supported by our ^{14}C dating: all the samples ages we obtained are younger than 15 kyr and belong to the last two epochs (Table 1).

The rates we obtain (12 ± 4 mm/yr, preferred minimum value of 11.6 ± 1.1 mm/yr) are thus consistent with the rate they inferred (11 ± 4 mm/yr) (Figure 8). *Liu and Zhou* [1986] found a slower rate (5 mm/yr), but their result was not constrained by measurement with a DEM and dating of offset geomorphic features. Other studies at sites on the eastern stretch of the Haiyuan fault, which ruptured during the 1920 earth-

quake (Plate 1), provided only lower bounds on the rate (8 ± 2 mm/yr [*Zhang et al.*, 1988a]; see discussion by *Gaudemer et al.* [1995, Figure 15a, pp. 639–640]) (Figure 8).

The range of slip amount per event ($8 \leq \Delta u \leq 16$ m) we derive from short-term offsets measured on one pair of stereoscopic HR photographs (site 4) and on total-station profiles (site 3) confirms the inference that great ($M_w \geq 8$) earthquakes rupture the Tianzhu gap [*Gaudemer et al.*, 1995]. Slip amounts of 8 to 16 m are compatible both with a slip rate of ~12 mm/yr and with the historical quiescence of the fault since at least 800 years [*Gaudemer et al.*, 1995]. They are in keeping with the 8 m average displacement observed during the $M = 8.7$ Haiyuan earthquake in 1920 [*Zhang et al.*, 1987]. Characteristic earthquakes with $\Delta u = 12 \pm 4$ m may occur on the Haiyuan fault, west of the Yellow River, since there is a record of successive earthquakes with similar individual offsets at two sites, a few kilometers apart, within the Tianzhu seismic gap. With a slip rate of 11.6 ± 1.1 mm/yr, the recurrence interval between such earthquakes would be of order of 1050 ± 450 years.

The combination of techniques we used (total-station profiling, stereoscopic analysis of high-resolution photographs, quantitative geomorphic reconstruction from digital elevation model), made possible by the pioneering implementation of a small remote-controlled, photogrammetric airplane, capable of taking-off, flying and landing in the field, should yield similarly useful results along large active faults in Central Asia, Tibet, and other remote areas of the world.

Acknowledgments. We thank Institut National des Sciences de l'Univers, Centre National de la Recherche Scientifique (Programme PNRN), Institut de Physique du Globe de Paris (BQR), and École Supérieure des Géomètres et Topographes (Le Mans) for encouraging and supporting both the development of the remote-controlled, photogrammetric airplane, and sustained work along the western Haiyuan fault. The Lawrence Livermore National Laboratory also provided financial support for ^{14}C dating. P. Tapponnier, M. Kasser, and Y. Gaudemer conceived the initial project of DEM acquisition through a transportable, field-adapted, small airplane. G. Dol piloted the airplane in the field. We are grateful to the China Seismological Bureau and the Lanzhou Seismological Institute for the excellent organization of logistics in the field. We are grateful to W. Bull and R. Yeats for careful reviews that improved the paper. We thank J. Van der Woerd for helpful discussion. This is IPGP contribution 1568 and INSU contribution 132.

References

Assaraj, A., Changements hydroclimatiques depuis 13000 ans BP au Tibet oriental et au nord de Xinjiang (Chine). Approche par l'étude de quelques enregistrements lacustres, Ph.D. thesis, Univ. Paris XI, Paris, France, 1997.

Avouac, J.-P., P. Tapponnier, M. Bai, H. You, and G. Wang, Active thrusting and folding along the northern Tien Shan and late Cenozoic rotation of the Tarim relative to Dzungaria and Kazakhstan, *J. Geophys. Res.*, *98*, 6755–6804, 1993.

Bull, W., *Geomorphic Responses to Climatic Change*, Oxford Univ. Press, New York, 1991.

Deng, Q., F. Song, S. Zhu, M. Li, T. Wang, W. Zhang, B. Burchfiel, P. Molnar, and P. Zhang, Active faulting and tectonics of the Ningxia-Hui autonomous region, China, *J. Geophys. Res.*, *89*, 4427–4445, 1984.

Deng, Q., et al., Variations in the geometry and amount of slip on the Haiyuan (Nanxihaushan) fault zone, China, and the surface rupture of the 1920 Haiyuan earthquake, in *Earthquake Source Mechanics, Geophys. Monogr. Ser.*, edited by Das, S. et al., vol. 37, pp. 169–182, AGU, Washington, D.C., 1986.

Gansu Geological Bureau, Geological map of Gansu, scale 1:1 000 000, Geol. Press, Beijing, 1975a.

Gansu Geological Bureau, Geological map of Gansu, scale 1:200 000, Geol. Press, Beijing, 1975b.

Gasse, F., J. Fontes, E. Van Campo, and K. Wei, Holocene environmental changes in lake Bangong Co basin (western Tibet), 4, discussion and conclusions, *Paleogeogr. Palaeoclimatol. Palaeoecol.*, *120*, 79–92, 1996.

Gasse, F., et al., A 13,000 year climate record from western Tibet, *Nature*, *353*, 742–745, 1991.

Gaudemer, Y., P. Tapponnier, B. Meyer, G. Peltzer, S. Guo, Z. Chen, H. Dai, and I. Cifuentes, Partitioning of crustal slip between linked active faults in the eastern Qilian Shan, and evidence for a major seismic gap, the 'Tianzhu gap', on the western Haiyuan fault, Gansu (China), *Geophys. J. Int.*, *120*, 599–645, 1995.

Gu, G., T. Lin, and Z. Shi, *Catalogue of Chinese Earthquakes (1831 BC–1969 AD)*, Science Press, Beijing, 1989.

Liu, B., and J. Zhou, The research on the active Haiyuan fault in China, *Northwest. Seismol. J.*, *8*, 79–88, 1986.

Liu, K. B., Z. Yao, and L. G. Thompson, A pollen record of Holocene climatic changes from the Dunde ice cap, Qinghai-Tibetan Plateau, *Geology*, *26*, 135–138, 1998.

Merritts, D. J., and K. R. Vincent, Geomorphic response of coastal streams to low, intermediate, and high rates of uplift, Mendocino triple junction region, northern California, *Geol. Soc. of Am. Bull*, *101*, 1373–1388, 1989.

Merritts, D. J., K. R. Vincent, and E. E. Wohl, Long river profiles, tectonism, and eustasy; a guide to interpreting fluvial terraces, *J. Geophys. Res.*, *99*, 14,031–14,050, 1994.

Meyer, B., P. Tapponnier, Y. Gaudemer, G. Peltzer, S. Guo, and Z. Chen, Rate of left-lateral movement along the easternmost segment of the Altyn Tagh fault, east of 96°E (China), *Geophys. J. Int.*, *124*, 29–44, 1996.

Meyer, B., P. Tapponnier, L. Bourjot, F. Métivier, Y. Gaudemer, G. Peltzer, S. Guo, and Z. Chen, Crustal thickening in Gansu-Qinghai, lithospheric mantle subduction, and oblique, strike-slip controlled growth of the Tibet Plateau, *Geophys. J. Int.*, *135*, 1–47, 1998.

Morel, P.-H., Étude photogrammétrique de la lacune sismique de la Fête Céleste, mémoire d'ingénieur, École Supér. des Géomètres et Topogr., Le Mans, France, 1995.

Pachur, H. J., B. Wünnemann, and Z. H., Lake evolution in the Tengger desert, northwestern China, during the last 40,000 years, *Quat. Res.*, *44*, 171–180, 1995.

Peltzer, G., P. Tapponnier, Z. Zhang, and Z. Q. Xu, Neogene and Quaternary faulting in and along the Qinling Shan, *Nature*, *317*, 500–505, 1985.

Peltzer, G., P. Tapponnier, Y. Gaudemer, B. Meyer, S. Guo, K. Yin, Z. Chen, and H. Dai, Offsets of late Quaternary morphology, rate of slip, and recurrence of large earthquakes on the Chang Ma fault (Gansu, China), *J. Geophys. Res.*, *93*, 7793–7812, 1988.

Personius, S. F., Late Quaternary stream incision and uplift in the forearc of the Cascadia subduction zone, western Oregon, *J. Geophys. Res.*, *100*, 20,193–20,210, 1995.

Repetti, W. C., The epicenter of the Kansu earthquake of May 23, 1927, *Bull. Seismol. Soc. Am.*, *18*, 1–14, 1928.

Scholz, C. H., Geophysics; earthquakes as chaos, *Nature*, *348*, 197–198, 1990.

Schwartz, D. P., and K. J. Coppersmith, Fault behavior and characteristic earthquakes; examples from the Wasatch and San Andreas faults zones, *J. Geophys. Res.*, *89*, 5681–5698, 1984.

Stuiver, M., and H. A. Polach, Discussion; reporting of ^{14}C data, *Radiocarbon*, *19*, 355–363, 1977.

Stuiver, M., and P. J. Reimer, Extended ^{14}C data base and revised CALIB 3.0 ^{14}C age calibration program, *Radiocarbon*, *35*, 215–230, 1993.

Tapponnier, P., and P. Molnar, Active faulting and tectonics in China, *J. Geophys. Res.*, *82*, 2905–2930, 1977.

Tapponnier, P., et al., Active thrusting and folding in the Qilian Shan, and decoupling between upper crust and mantle in northeastern Tibet, *Earth. Planet. Sci. Lett.*, *97*, 382–403, 1990.

Van Campo, E., and F. Gasse, Pollen- and diatom-inferred climatic and hydrological changes in Sumxi Co basin (western Tibet) since 13,000 yr B.P., *Quat. Res.*, *39*, 300–313, 1993.

Van der Woerd, J., F. J. Ryerson, P. Tapponnier, Y. Gaudemer, R. Finkel, A. S. Mériaux, M. Caffee, G. Zhao, and Q. He, Holocene left-slip rate determined by cosmogenic surface dating on the Xidatan segment of the Kunlun fault (Qinghai, China), *Geology*, *26*, 695- 698, 1998.

Weldon, R. J., The Late Cenozoic geology of Cajon Pass. Implications for tectonics and sedimentation along the San Andreas fault, Ph.D. thesis, Calif. Inst. of Technol., Pasadena, 1986.

Weldon, R. J., and K. E. Sieh, Holocene rate of slip and tentative recurrence interval for large earthquakes on the San Andreas fault, Cajon Pass, southern California, *Geol. Soc. of Am. Bull*, *96*, 793–812, 1985.

Wells, D. L., and K. J. Coppersmith, New empirical relationships among magnitude, rupture length, rupture width, rupture area, and surface displacement, *Bull. Seismol. Soc. Am.*, *84*, 974–1002, 1994.

Xu, W., Y. He, and Y. Yan, Tectonic characteristics and hydrocarbons of the Hexi Corridor, in *Chinese Sedimentary Basins*, edited by X. Zhu, pp. 53–63, Elsevier, New York, 1989.

Zhang, P., P. Molnar, B. C. Burchfiel, L. H. Royden, Y. Wang, Q. Deng, F. Song, W. Zhang, and D. Jiao, Bounds on the Holocene slip rate of the Haiyuan fault, north-central china, *Quat. Res.*, *30*, 151–164, 1988a.

Zhang, P., P. Molnar, W. Zhang, Q. Deng, Y. Wang, B. C. Burchfiel, F. Song, L. H. Royden, and D. Jiao, Bounds on the average recurrence interval of major earthquakes along the Haiyuan fault in north-central China, *Seismol. Res. Lett.*, *59*, 81–89, 1988b.

Zhang, W., D. Jiao, P. Zhang, P. Molnar, B. C. Burchfiel, Q. Deng, Y. Wang, and F. Song, Displacement along the Haiyuan fault associated with the great 1920 Haiyuan, China, earthquake, *Bull. Seismol. Soc. Am.*, *77*, 117–131, 1987.

Zhang, Y. Q., P. Vergely, and J. Mercier, Active faulting in and along the Qinling Range (China) inferred from SPOT imagery analysis and extrusion tectonics of south China, *Tectonophysics*, *243*, 69–95, 1995.

Y. Gaudemer, G. C. P. King, C. Lasserre, F. Métivier and P. Tapponnier, Institut de Physique du Globe de Paris, CNRS UMR 7578, 4, place Jussieu, 75252 Paris Cédex 05, France. (e-mail: gaudemer@ipgp.jussieu.fr; king@ipgp.jussieu.fr; lasserre@ipgp.jussieu.fr; metivier@ipgp.jussieu.fr; tappon@ipgp.jussieu.fr)

M. Kashgarian and F. J. Ryerson, Lawrence Livermore National Laboratory, P.O. Box 808, L202, Livermore, CA 94551, USA. (e-mail: ryerson@s91.es.llnl.gov)

M. Kasser and P.-H. Morel, École Supérieure des Géomètres et Topographes, 1, Bd Pythagore, 72000 Le Mans, France. (e-mail: kasser@esgt.cnam.fr)

Liu B., Lu T. and Yuan D., Seismological Institute of Lanzhou, CSB, Lanzhou, Gansu 730000, P.R. China.

(Received June 1, 1998; revised October 29, 1998; accepted November 6, 1998.)